



|                               |   |
|-------------------------------|---|
| <b>Publication Year</b>       | 2017  |
| <b>Acceptance in OA @INAF</b> | 2020-09-03T15:54:07Z  |
| <b>Title</b>                  | F-GAMMA: variability Doppler factors of blazars from multiwavelength monitoring                 |
| <b>Authors</b>                | Liodakis, I.; MARCHILI, Nicola; Angelakis, E.; Fuhrmann, L.; Nestoras, I.; et al.               |
| <b>DOI</b>                    | 10.1093/mnras/stx002  |
| <b>Handle</b>                 | <a href="http://hdl.handle.net/20.500.12386/27113">http://hdl.handle.net/20.500.12386/27113</a> |
| <b>Journal</b>                | MONTHLY NOTICES OF THE ROYAL ASTRONOMICAL SOCIETY   |
| <b>Number</b>                 | 466   |



# F-GAMMA: variability Doppler factors of blazars from multiwavelength monitoring

I. Liodakis,<sup>1,2★</sup> N. Marchili,<sup>3</sup> E. Angelakis,<sup>4</sup> L. Fuhrmann,<sup>4,5</sup> I. Nestoras,<sup>4</sup>  
I. Myserlis,<sup>4</sup> V. Karamanavis,<sup>4</sup> T. P. Krichbaum,<sup>4</sup> A. Sievers,<sup>6</sup> H. Ungerechts<sup>6</sup>  
and J. A. Zensus<sup>4</sup>

<sup>1</sup>Department of Physics and ITCP,<sup>1</sup> University of Crete, 71003 Heraklion, Greece

<sup>2</sup>Foundation for Research and Technology – Hellas, IESL, Voutes, 7110 Heraklion, Greece

<sup>3</sup>IAPS–INAF, Via Fosso del Cavaliere 100, I-00133 Roma, Italy

<sup>4</sup>Max-Planck-Institut für Radioastronomie, Auf dem Hügel 69, D-53121 Bonn, Germany

<sup>5</sup>ZESS – Center for Sensorsystems, University of Siegen, Paul-Bonatz-Str. 9-11, D-57076 Siegen, Germany

<sup>6</sup>Instituto de Radio Astronomía Milimétrica, Avenida Divina Pastora 7, Local 20, E-18012 Granada, Spain

Accepted 2017 January 3. Received 2016 December 14; in original form 2016 May 13

## ABSTRACT

Recent population studies have shown that variability Doppler factors can describe blazars as a population adequately. We use the flux-density variations found within the extensive radio multiwavelength data sets of the F-GAMMA programme, a total of 10 frequencies from 2.64 up to 142.33 GHz, in order to estimate the variability Doppler factors for 58  $\gamma$ -ray bright sources, for 20 of which no variability Doppler factor has been estimated before. We employ specifically designed algorithms in order to obtain a model for each flare at each frequency. We then identify each event and track its evolution through all the available frequencies for each source. This approach allows us to distinguish significant events producing flares from stochastic variability in blazar jets. It also allows us to constrain effectively the variability brightness temperature and hence the variability Doppler factor, as well as error estimates. Our method can produce the most accurate (16 per cent error, on average) estimates in the literature to date.

**Key words:** Physical data and processes: relativistic processes – galaxies: active – BL Lacertae objects: general – galaxies: jets.

## 1 INTRODUCTION

Blazars, the subclass of active galactic nuclei (AGN) with their jet axis pointing towards us, include flat-spectrum radio quasars (FSRQs) and BL Lac objects, which dominate the  $\gamma$ -ray extragalactic sky. Blazars are characterized by extremely broad-band emission (from long cm radio wavelengths to TeV energies), intense variability at all wavelengths, relativistic boosting of the emitted luminosity and often significantly apparent superluminal motion. Most of these exotic phenomena are attributed to the combination of relativistic speeds and the alignment of the jet to our line of sight (Blandford & Königl 1979), which obscures our view of their intrinsic properties. The observed properties of blazar jets are modulated by the Doppler factor, defined as  $\delta = [\Gamma(1 - \beta \cos \theta)]^{-1}$ , where  $\Gamma = (\sqrt{1 - \beta^2})^{-1}$  is the Lorentz factor,  $\beta$  the velocity of the jet in units of the speed of light and  $\theta$  the jet viewing angle.

As  $\delta$  is one of the most important parameters in the blazar paradigm, many methods have been proposed for estimating it. Such methods are equipartition Doppler factors (Readhead 1994; Gujosa & Daly 1996), variability Doppler factors (Lähteenmäki & Valtaoja 1999; Valtaoja et al. 1999) and single-component causality Doppler factors (Jorstad et al. 2005, 2006), as well as inverse Compton Doppler factors (Ghisellini et al. 1993) and  $\gamma$ -ray opacity Doppler factors (Mattox et al. 1993; Dondi & Ghisellini 1995). Equipartition and variability Doppler factors are based on the assumption of equipartition between the energy density of the magnetic field and the radiating particles (Readhead 1994). The former uses the brightness temperature measured from very-long-baseline interferometry (VLBI) observations, the latter the variability brightness temperature from flux-density variations. The single-component causality Doppler factor method uses the observed angular size and variability time-scale to calculate the Doppler factor for each individual component. The Doppler factor of a source is then calculated as the weighted mean of the Doppler factors of all the components, with weights inversely proportional to the uncertainty in the apparent velocity of each component. Inverse

★ E-mail: liodakis@physics.uoc.gr

Compton Doppler factors use the framework of the synchrotron self-Compton (SSC) model in order to estimate the expected X-ray flux density, given the angular size and flux density of the core from VLBI observations. The Doppler factor is obtained by comparing the observed and theoretically expected X-ray flux density.  $\gamma$ -ray opacity Doppler factors use pair-production absorption effects, resulting from the interaction of  $\gamma$ - and X-rays. Assuming that the emission region has a spherical geometry, X-rays and  $\gamma$ -rays are cospatial and the region is transparent to  $\gamma$ -rays, a lower limit on the Doppler factor can be obtained by relating the variability time-scale to the size of the emission region.

Each one of the above methods uses different assumptions, which might not hold. Thus a direct comparison of the results from different methods is unable to provide the answer as to which method can describe blazars best. Recent population models (Liodakis & Pavlidou 2015a) have shown that the variability Doppler factor method (Lähtenmäki & Valtaoja 1999; Lähtenmäki, Valtaoja & Wiik 1999; Valtaoja et al. 1999; Hovatta et al. 2009) can describe both FSRQ and BL Lac populations adequately (Liodakis & Pavlidou 2015b), although application on a source-by-source basis has to be performed with caution. Moreover, an error analysis has shown that, although it is the most accurate (30 per cent error on average for each estimate), it suffers from systematics introduced due to the cadence of observations. Since the method involves fitting the flux density radio light curves with exponentials (in order to calculate the variability time-scale, flare amplitude and then the variability brightness temperature), flares faster than the cadence of observations will be unresolved, setting an upper limit on the fastest observed time-scale and thus the Doppler factor. We can overcome such a limitation in two ways: either by using data from surveys with high cadence observations, such as the Owens Valley Radio Observatory (OVRO)<sup>2</sup> blazar programme (Richards et al. 2011), or, as in our case, by modelling the flares.

In this work we use the extensive eight-year-long multi-wavelength radio light curves from the F-GAMMA programme<sup>3</sup> (Fuhrmann et al. 2007; Angelakis et al. 2010, 2012; Fuhrmann et al. 2016). The F-GAMMA programme monitored a sample of powerful and variable sources detected by the *Fermi* gamma-ray space telescope<sup>4</sup> (Acero et al. 2015) at ten frequencies from 2.64 up to 142.33 GHz with an approximately monthly cadence (sparse data sets at 228.9 and 345 GHz are also available). Our goals were to distinguish significant events occurring in blazar jets from stochastic variations and effectively constrain the variability parameters of each source, in order to estimate their variability Doppler factors. The method we use to estimate variability Doppler factors is described in detail in Angelakis et al. (2015). For the purposes of the current work, an error estimation step has been added in our analysis pipeline.

The article is organized as follows. In Section 2, we give a short description of the methods used. In Section 3, we present our estimates for the variability Doppler factors, Lorentz factors and viewing angles of the sources in our sample and in Section 4 a comparison with estimates from the literature, which we use as a proxy to validate our estimates; in Section 5 we summarize our results.

The cosmological parameters we adopt in this work are  $H_0 = 71 \text{ km s}^{-1} \text{ Mpc}^{-1}$ ,  $\Omega_m = 0.27$  and  $\Omega_\Lambda = 1 - \Omega_m$  (Komatsu et al. 2009).

## 2 METHODS

The calculation of the variability brightness temperatures and Doppler factors of our sources depends on the estimation of their variability characteristics, i.e. the amplitude and time-scales of the corresponding flares. The variability characteristics of multiple flares have been evaluated for 58 sources of the F-GAMMA sample using the flare decomposition method of Angelakis et al. (2015). With the addition of an error-analysis step, the method now consists of four steps.

(i) **Flare modelling.** This step of the method aims at identifying one basic flare pattern common among all events. The operation is executed separately for source and frequency. At first, all the flares in the light curve need to be localized by the identification of local maxima. Because flares appear at different times and with different amplitudes, the detected events are shifted in time and scaled in flux density, so that eventually they are all superimposed on the most prominent event. A lower envelope is then fitted to the pattern that has resulted from this stacking. It is this envelope that we consider as the template flare itself for further analysis.

(ii) **Correlation.** This operation aims at finding the optimum time delays between events at different frequencies. Instead of using a standard cross-correlation function (e.g. Edelson & Krolik 1988; Lehar et al. 1992), which would treat one pair of light curves each time, we include them all simultaneously. A cumulative correlation degree is calculated by multiplying the cross-correlation coefficients of all light-curve pairs after applying to them different time shifts. The set of time shifts that returns the highest degree of cumulative correlation defines the optimum average time delays among frequencies. Clearly, the more frequencies available, the more accurate the estimate of the time shifts.

(iii) **Flare characterization.** Using the temporal information from the previous step (correlation), this step is meant to identify and characterize the flares that are visible at multiple frequencies, using the model from the first step (flare modelling). The identification of flares at multiple frequencies ensures that only significant events are taken into account. Since the frequency availability is not constant, the number of required frequencies for an event is not strict and it is decided empirically. From the flare decomposition, we can calculate the variability time-scale and amplitude of each flare, which can be used for computation of the variability brightness temperature at each frequency (equation 1).

(iv) **Error analysis.** This operation is meant to provide an estimate of the uncertainty in the flare characteristics. Both amplitude and time-scales are affected by some degree of uncertainty. This uncertainty can be assessed by changing the basic shape of the flare models (both their duration and amplitude) and then repeating the flare characterization using the modified flare models. With each model we associate a goodness of fit, provided by the standard deviation of residuals. All models for which this value exceeds the goodness of fit of the best model by more than 10 per cent are disregarded. The range of flare time-scales and amplitudes for acceptable models sets our uncertainty and what we quote as the error of our estimates.

Figs 1 and 2 show some examples of simulated light curves (having subtracted the baseline) created after the modelling procedure has been completed. OJ287 (Fig. 1, upper panel) and 0716+714 (Fig. 1, lower panel) are among the fastest sources in our sample; it appears that our method can trace their flux-density variations well. The analysis of J0050–0929 (Fig. 2, upper panel), which shows slow variability, is similarly efficient. However, the case of

<sup>2</sup> <http://www.astro.caltech.edu/ovroblazars/>

<sup>3</sup> <http://www3.mpifr-bonn.mpg.de/div/vlbi/fgamma/fgamma.html>

<sup>4</sup> <http://fermi.gsfc.nasa.gov/>

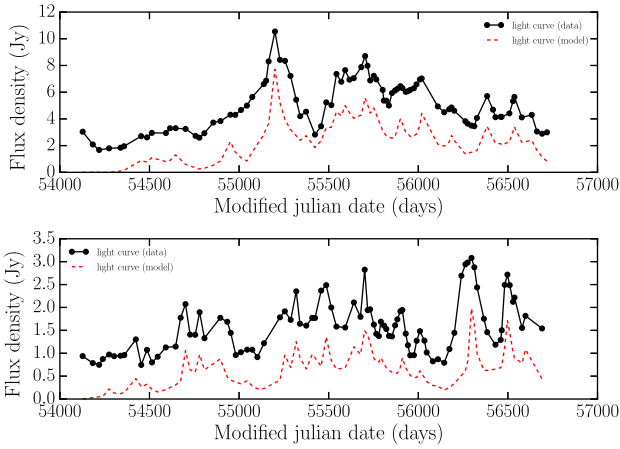


**Figure 1.** Observed (solid black) and simulated (dashed red) light curves for OJ287 (15 GHz, upper panel) and J0721+7120 (10.45 GHz, lower panel) after the flare modelling procedure has been completed.

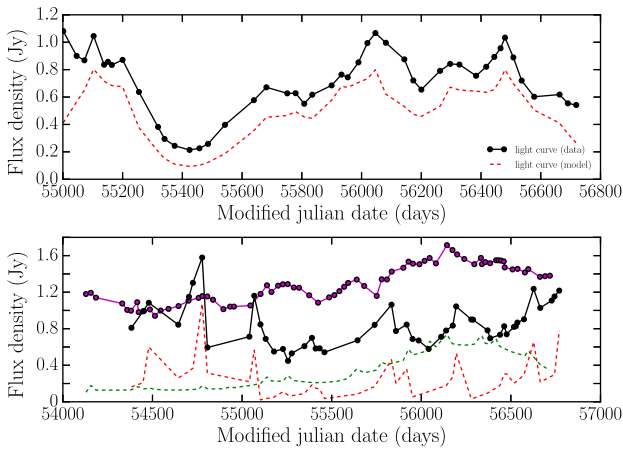


**Figure 2.** Observed (solid black) and simulated (dashed red) light curves for J0050–0929 (8.35 GHz, upper panel) and J0241–0815 (142.33 GHz solid black and dashed red, 10.45 GHz solid magenta and dashed green) after the flare modelling procedure has been completed.

J0241–0815 (Fig. 2, lower panel) is less clear: although we can trace the variability at individual frequencies well, the significant differences in the variability characteristics at different frequencies make it hard to trace the evolution of single flares efficiently.

The sources analysed have been classified according to the quality of their analysis results into three categories: very confident, confident and less confident. The first category includes sources with variability characteristics, along with sampling rate, that allow us to clearly identify and trace the evolution of flares across all available frequencies. The second category includes sources for which some difficulties have been encountered in modelling the light curves; these difficulties (e.g. a gap in the data, high noise in a minority of frequencies) are expected to have mild effects on the estimation of the variability characteristics. Results for sources of the third category should be regarded as the least reliable, because of poor sampling, noisy data or few available frequencies.

Multiwavelength modelling of flares provides several advantages over a simple fit. Examining the light curves at different frequencies provides valuable information regarding the evolution of the flares, the type of variability in the source (fast or slow) and the quality

of each data set. This information is taken into account during flare modelling.

In addition, the simultaneous use of all light curves allows us to mitigate the issues related to both the cadence of observations and the superposition of multiple flares. This is obtained by exploiting the general decrease of time-scales with frequency. Sources with very fast variability can be modelled best at low frequencies, allowing us to trace back the probable location of flares at high frequency, even below the cadence of observations. In contrast, flares in slowly varying sources can be recognized best at the highest frequencies; knowing their spectral evolution, we can roughly estimate the contribution of each flare to the variability observed at low frequencies, where, due to the long time-scales, single flares cannot easily be isolated. Examples of multiwavelength light curves can be found in Angelakis et al. (2010, 2012) and Fuhrmann et al. (2016) and on the F-GAMMA website.<sup>5</sup>

Given the above considerations, our flare characterization is limited by the cadence of observations at the lowest frequencies. The F-GAMMA sources have a sampling of  $\sim 30$  d and, in some cases (sources known to show significant variability, e.g. PKS 0716+714),  $\sim 14$  d. Given the typical blazar variability time-scales in the radio, multiwavelength information and the method’s ability to mitigate the effects of the observing cadence, it is rather unlikely that any significant event during the F-GAMMA monitoring period has not been accounted for. However, if there are sources in our sample that show variability at time-scales significantly shorter than  $\sim 14$  d, our results should be treated with caution.

### 3 VARIABILITY DOPPLER FACTORS

Once the flares have been identified and modelled, their variability characteristics can be estimated. Their amplitude coincides with the flux density at the peak. The time-scales of a flare are the time spans between the beginning of the flare and its peak and between the peak and its end. We define the beginning of a flare as the time at which its flux density exceeds a threshold of 0.25 times the average uncertainty in the flux-density measurements. The end of a flare is defined similarly, as the time when the flux density drops below that threshold. This definition helps in dealing with flares that extend to very long time-scales without carrying any significant contribution to the total flux density.

Through the variability characteristics of flares, the associated variability brightness temperatures can be calculated using the following formula:

$$T_{\text{var}} = 1.47 \times 10^{13} \frac{D_L^2 \Delta S_{\text{ob}}(\nu)}{\nu^2 t_{\text{var}}^2 (1+z)^4}, \quad (1)$$

where  $T_{\text{var}}$  is the variability brightness temperature in Kelvin,  $D_L$  is the luminosity distance in Mpc,  $S_{\text{ob}}(\nu)$  the flux density in Jy,  $t_{\text{var}}$  the variability time-scale in days,  $z$  the redshift and  $\nu$  the observing frequency in GHz. The numerical factor is related to units and the geometry of the emitting region. Assuming that while flaring, sources reach equipartition (Readhead 1994), the intrinsic brightness temperature will be equal to the equipartition brightness temperature  $T_{\text{eq}} = 5 \times 10^{10}$  K (Readhead 1994; Lähteenmäki et al. 1999). By

<sup>5</sup> <http://www3.mpifr-bonn.mpg.de/div/vlbi/fgamma/fgamma.html>

comparing the observed and intrinsic brightness temperature, we estimate the variability Doppler factor as follows:

$$\delta_{\text{var}} = (1 + z) \sqrt[3]{\frac{T_{\text{var}}}{T_{\text{eq}}}}. \quad (2)$$

For the full derivation of equation (2), see Appendix A. The highest variability brightness temperature observed in a source provides the highest constraint on the variability Doppler factor. The highest estimate for the variability Doppler factor found in each source is the estimate we quote in Table 1.

We calculate the Lorentz factor ( $\Gamma_{\text{var}}$ ) and viewing angle ( $\theta_{\text{var}}$ ) using equations (3) and (4) and the apparent velocity ( $\beta_{\text{app}}$ ). In order to estimate the mean  $\beta_{\text{app}}$ , we use data from the Monitoring Of Jets in Active galactic nuclei with Very Long Baseline Array Experiments (MOJAVE) survey (Lister & Homan 2005) for all our sources with available estimates in the literature (Lister et al. 2009, 2013):

$$\Gamma_{\text{var}} = \frac{\beta_{\text{app}}^2 + \delta_{\text{var}}^2 + 1}{2\delta_{\text{var}}}, \quad (3)$$

$$\theta_{\text{var}} = \arctan \frac{2\beta_{\text{app}}}{\beta_{\text{app}}^2 + \delta_{\text{var}}^2 - 1}. \quad (4)$$

All estimates for the Doppler factors as well as the Lorentz factors and viewing angles are summarized in Table 1. It is obvious that the more flares and frequencies used for the characterization of the light curves, the better we can constrain the variability brightness temperature and the more confident we are about the results of our analysis. The number in the last column of Table 1 (column 13) denotes our confidence in the estimate. 0 denotes cases for which we are less confident in the results of our analysis, 1 cases in which we are confident and 2 cases in which we are very confident. The confidence in the estimate of the Doppler factor depends on the abundance of data points available for each source. Sparse data, large observational gaps or fewer available frequencies could severely hamper evolution tracking and characterization of the flares, which is the basis of our methodology. Such problems in the analysis could lead to underestimation of the variability brightness temperature. An additional cause for our lack in confidence would be a general lack of flares in a source. For a discussion and notes on the analysis of individual sources, see Marchili et al. (in preparation). A more conservative approach to the equipartition brightness temperature would be to use the inverse Compton catastrophe limit  $T_{\text{IC}} = 10^{12}$  K (Kellermann & Pauliny-Toth 1969). This would bring our estimates lower by a factor of  $\sim 2.7$ . We chose to use the equipartition limit, since the variability Doppler factors using equipartition (Hovatta et al. 2009) best describe the blazar populations (Liodakis & Pavlidou 2015b).

Fig. 3 shows the distribution of variability Doppler factors, Fig. 4 the distribution of Lorentz factors and Fig. 5 the distribution of viewing angles for the F-GAMMA sources, where solid red is for FSRQs, dashed green for BL Lacs and dotted blue for radio galaxies. FSRQs and BL Lacs (except for two BL Lacs) have viewing angles lower than  $15^\circ$ , consistent with the current view of blazars (Ghisellini et al. 1993; Urry & Padovani 1995). The values for the mean and standard deviation (std) of the populations are summarized in Table 2.

The FSRQs appear to have higher Doppler factors than the BL Lacs and both are higher than the radio galaxies, as expected. The same is the case for Lorentz factors and the opposite for viewing angles. The highest Lorentz factor is attributed to the BL Lac object J1824+5651; this estimate, however, falls within the category of ‘less confident’ results. The high Lorentz factor that we found for

this source may be caused by an underestimation of the Doppler factor ( $\delta_{\text{var}} = 1$ ). A higher Doppler factor estimate (even  $\delta_{\text{var}} = 2$ ) would bring the value of the Lorentz factor lower than that of the fastest FSRQs with estimates labelled ‘confident’ and ‘very confident’ (J0423–0120  $\Gamma_{\text{var}} = 22.2$  and J2025–0735  $\Gamma_{\text{var}} = 24.6$ , respectively).

The mean value for the Doppler factor for the ‘confident’ and ‘very confident’ estimates ( $\sim 14$ ) is very similar to the overall mean ( $\sim 12$ ). Thus we can conclude that the reliability of the estimates (in these two categories) does not influence the results of our analysis strongly. However, for the ‘less confident’ estimates, the mean is  $\sim 6$  while the mean of the apparent velocity (7.6) is similar to the sample mean (8.3), as is the case for the ‘confident’ and ‘very confident’ categories. The resulting  $\Gamma_{\text{var}}$  and  $\theta_{\text{var}}$  for the ‘less confident’ estimates are larger than those of the sample. There are two possible explanations for this discrepancy. Either there are indeed unaccounted-for peculiarities of the analysis that lead to underestimation of the Doppler factor for these sources or the majority of the sources labelled ‘less confident’ are slowly variable. In the latter case, their Doppler factors will be low, causing an increase in the value of the Lorentz factor. In that case, the source composition of the category is biasing the results. In either case, estimates labelled as ‘less confident’ should be treated with caution.

In order to assess the significance of possible differences between FSRQs and BL Lacs in our sample, we use the Wilcoxon rank-sum test, which gives the probability of two samples having been drawn from the same distribution (the alternative hypothesis is that values from one sample are more likely to be larger than the other). The probability of the two samples being drawn from the same distribution is 1.1 per cent for variability Doppler factors, 0.3 per cent for Lorentz factors and 4.9 per cent for viewing angles. Although we cannot reach solid conclusions for the populations, this would imply that FSRQs have on average higher Doppler factors and Lorentz factors and smaller viewing angles than BL Lacs (Jorstad et al. 2005; Hovatta et al. 2009; Lister et al. 2013; Liodakis & Pavlidou 2015a).

Fig. 6 shows the distribution of the errors in our estimates (upper panel) and the error of each estimate against the value of the Doppler factor (lower panel). The mean of the error distribution for the whole sample is 2.07, with a standard deviation of 1.99. The highest percentage error in our estimates is 35.5 per cent, which is comparable to the most accurate estimates available in the literature ( $\sim 30$  per cent error on average) as derived from population models. Overall, our method has a 16 per cent error on average, making our method the most accurate approach to date.

## 4 COMPARISON WITH OTHER METHODS

The F-GAMMA sample is not flux-limited or complete and hence our results (drawn from it) cannot be statistically tested against blazar population models. We can, however, use as a proxy estimates that have been shown to be consistent with the population. We chose to compare our Doppler factors with Hovatta et al. (2009) for two reasons: (a) it is the most recent study on variability Doppler factors using a different approach for estimating the variability brightness temperature; (b) estimates from Hovatta et al. (2009) have been tested against population models (Liodakis & Pavlidou 2015b) and it was shown that they can describe both the FSRQ and BL Lac populations adequately.

Fig. 7 shows the comparison between the variability Doppler factors derived in this work and those from Hovatta et al. (2009). The two samples have 38 sources in common. In Hovatta et al. (2009), the authors comment on how difficult is to determine the

**Table 1.** Variability Doppler factors, Lorentz factors and viewing angles for the F-GAMMA sample. Column (1) is the F-GAMMA identification, (2) alternative source name, (3) class (B is for BL Lacs, Q for FSRQs and G for radio galaxies), (4) redshift, (5) variability Doppler factor, (6) error in the variability Doppler factor (7) Lorentz factor, (8) viewing angle, (9) mean apparent velocity, (10) number of flares characterized, (11) number of frequencies used for the calculation, (12) frequency that gave the highest estimate of the variability Doppler factor and (13) confidence in the Doppler factor (0 denotes estimates for which we are less confident in our analysis, 1 estimates for which we are confident and 2 estimates for which we are very confident in our analysis).

| F-GAMMA<br>(ID) | Alt. name    | Class | $z$   | $\delta_{\text{var}}$ | $\sigma_{\delta_{\text{var}}}$ | $\Gamma$ | $\theta$ (deg.) | $\beta_{\text{app}}$ | No<br>flares | No<br>freq. | $\nu$ (GHz) | Conf. |
|-----------------|--------------|-------|-------|-----------------------|--------------------------------|----------|-----------------|----------------------|--------------|-------------|-------------|-------|
| J0050–0929      | 0048–097     | B     | 0.634 | 12.8                  | 3.4                            | –        | –               | –                    | 7            | 9           | 2.64        | 2     |
| J0102+5824      | 0059+5808    | Q     | 0.644 | 21.9                  | 3.6                            | 12.0     | 1.5             | 6.89                 | 8            | 9           | 2.64        | 2     |
| J0136+4751      | 0133+476     | Q     | 0.859 | 13.7                  | 2.7                            | 9.5      | 3.7             | 8.43                 | 4            | 7           | 8.35        | 2     |
| J0217+0144      | PKS0215+015  | Q     | 1.715 | 27.1                  | 1.3                            | 19.1     | 1.9             | 17.30                | 7            | 9           | 2.64        | 2     |
| J0222+4302      | B0219+428    | B     | 0.444 | 4.3                   | 0.2                            | –        | –               | –                    | 3            | 9           | 2.64        | 1     |
| J0237+2848      | 0234+285     | Q     | 1.206 | 12.2                  | 4.3                            | 14.9     | 4.6             | 14.65                | 4            | 9           | 2.64        | 2     |
| J0238+1636      | 0235+164     | B     | 0.940 | 29.0                  | 7.7                            | 14.6     | 0.3             | 2.00                 | 7            | 9           | 2.64        | 2     |
| J0241–0815      | 0238–084     | G     | 0.005 | 0.3                   | 0.0                            | 2.0      | 26.9            | 0.22                 | 6            | 8           | 8.35        | 0     |
| J0336+3218      | PKS0333+321  | Q     | 1.259 | 2.9                   | 0.2                            | 21.4     | 10.0            | 10.66                | 4            | 2           | 86.00       | 0     |
| J0339–0146      | 0336–019     | Q     | 0.850 | 16.7                  | 3.5                            | 12.2     | 3.2             | 11.34                | 5            | 9           | 4.85        | 0     |
| J0359+5057      | 0355+50      | Q     | 1.520 | 26.3                  | 3.6                            | 13.2     | 0.2             | 1.39                 | 4            | 10          | 2.64        | 1     |
| J0418+3801      | B20415+37    | G     | 0.049 | 2.0                   | 0.4                            | 7.0      | 20.0            | 4.85                 | 6            | 9           | 2.64        | 2     |
| J0423–0120      | 0420–014     | Q     | 0.916 | 43.9                  | 9.2                            | 22.2     | 0.3             | 4.44                 | 8            | 9           | 2.64        | 1     |
| J0433+0521      | 0430+052     | G     | 0.033 | 2.1                   | 0.1                            | 6.8      | 19.9            | 4.81                 | 4            | 9           | 4.85        | 1     |
| J0530+1331      | 0528+134     | Q     | 2.070 | 12.9                  | 2.5                            | 10.8     | 4.4             | 10.50                | 5            | 7           | 8.35        | 2     |
| J0654+4514      | S40650+453   | Q     | 0.928 | 13.8                  | 2.6                            | –        | –               | –                    | 6            | 9           | 14.6        | 2     |
| J0719+3307      | TXS0716+332  | Q     | 0.779 | 14.1                  | 0.5                            | –        | –               | –                    | 5            | 7           | 2.64        | 0     |
| J0721+7120      | 0716+714     | B     | 0.328 | 14.0                  | 0.9                            | 10.8     | 3.9             | 10.22                | 14           | 10          | 2.64        | 2     |
| J0730–1141      | PKS0727–115  | Q     | 1.591 | 39.8                  | 6.9                            | –        | –               | –                    | 7            | 9           | 2.64        | 2     |
| J0738+1742      | 0735+178     | B     | 0.424 | 4.5                   | 0.4                            | 3.6      | 12.2            | 3.30                 | 3            | 9           | 4.85        | 1     |
| J0808–0751      | 0805–077     | Q     | 1.837 | 14.9                  | 1.2                            | 24.3     | 3.5             | 22.42                | 4            | 9           | 8.35        | 2     |
| J0818+4222      | 0814+425     | B     | 0.530 | 7.8                   | 2.6                            | 4.1      | 3.2             | 1.72                 | 5            | 9           | 23.05       | 1     |
| J0824+5552      | S40820+560   | Q     | 1.417 | 2.4                   | 0.5                            | –        | –               | –                    | 4            | 2           | 86.00       | 0     |
| J0841+7053      | 0836+710     | Q     | 2.218 | 12.1                  | 0.0                            | 19.0     | 4.4             | 17.69                | 1            | 9           | 2.64        | 0     |
| J0854+2006      | 0851+202     | B     | 0.306 | 8.7                   | 1.1                            | 7.6      | 6.6             | 7.49                 | 10           | 10          | 4.85        | 2     |
| J0920+4441      | S40917+449   | Q     | 2.190 | 5.0                   | 0.9                            | 2.8      | 6.2             | 1.45                 | 1            | 8           | 4.85        | 0     |
| J0958+6533      | 0954+658     | B     | 0.367 | 10.7                  | 1.7                            | 7.9      | 5.0             | 7.31                 | 9            | 9           | 2.64        | 2     |
| J1104+3812      | PKS1101+384  | B     | 0.030 | 1.7                   | 0.1                            | 1.1      | 8.6             | 0.14                 | 6            | 9           | 2.64        | 2     |
| J1130–1449      | 1127–145     | Q     | 1.184 | 21.9                  | 0.0                            | 13.0     | 1.9             | 9.46                 | 4            | 8           | 4.85        | 1     |
| J1159+2914      | PKS1156+295  | Q     | 0.725 | 12.8                  | 0.0                            | 16.6     | 4.3             | 16.13                | 6            | 9           | 2.64        | 2     |
| J1217+3007      | PKS1215+303  | B     | 0.130 | 1.1                   | 0.3                            | 1.0      | 20.7            | 0.03                 | 3            | 8           | 86.00       | 0     |
| J1221+2813      | QSOB1219+285 | B     | 0.102 | 2.6                   | 0.6                            | 4.6      | 19.8            | 4.08                 | 5            | 8           | 2.64        | 1     |
| J1229+0203      | 1226+023     | Q     | 0.158 | 3.7                   | 1.0                            | 12.0     | 11.3            | 8.58                 | 6            | 8           | 8.35        | 1     |
| J1256–0547      | 1253–055     | Q     | 0.536 | 16.8                  | 2.9                            | 12.3     | 3.2             | 11.42                | 9            | 9           | 23.05       | 1     |
| J1310+3220      | 1308+326     | B     | 0.997 | 15.8                  | 1.7                            | 17.1     | 3.6             | 16.99                | 6            | 9           | 2.64        | 1     |
| J1332–0509      | PKS1329–049  | Q     | 2.150 | 18.9                  | 3.9                            | 11.1     | 2.1             | 7.70                 | 6            | 8           | 4.85        | 1     |
| J1504+1029      | 1502+106     | Q     | 1.839 | 17.3                  | 2.7                            | 11.4     | 2.8             | 9.63                 | 5            | 10          | 4.85        | 2     |
| J1512–0905      | 1510–089     | Q     | 0.360 | 12.3                  | 2.8                            | 19.0     | 4.4             | 17.76                | 10           | 9           | 2.64        | 2     |
| J1613+3412      | 1611+343     | Q     | 1.400 | 2.4                   | 0.5                            | 31.5     | 9.2             | 11.93                | 3            | 2           | 86.00       | 0     |
| J1635+3808      | 1633+382     | Q     | 1.814 | 20.3                  | 2.8                            | 14.9     | 2.6             | 13.78                | 8            | 10          | 8.35        | 2     |
| J1642+3948      | 1641+399     | Q     | 0.593 | 10.4                  | 2.9                            | 11.3     | 5.5             | 11.22                | 6            | 9           | 2.64        | 2     |
| J1653+3945      | 1652+398     | B     | 0.033 | 2.1                   | 0.0                            | 1.3      | 8.2             | 0.24                 | 5            | 9           | 2.64        | 0     |
| J1733–1304      | PKS1730–130  | Q     | 0.902 | 17.6                  | 3.4                            | 15.3     | 3.2             | 15.09                | 7            | 10          | 42.00       | 0     |
| J1751+0939      | 1749+096     | B     | 0.322 | 14.2                  | 2.0                            | 7.8      | 2.3             | 4.36                 | 9            | 9           | 2.64        | 2     |
| J1800+7828      | 1803+784     | B     | 0.680 | 21.2                  | 5.0                            | 10.8     | 0.6             | 2.53                 | 8            | 9           | 2.64        | 2     |
| J1824+5651      | 1823+568     | B     | 0.664 | 1.0                   | 0.2                            | 34.8     | 13.4            | 8.36                 | 5            | 1           | 86.00       | 0     |
| J1848+3219      | TXS1846+322  | Q     | 0.798 | 12.1                  | 1.4                            | 7.0      | 3.2             | 4.69                 | 7            | 9           | 2.64        | 2     |
| J1849+6705      | S41849+670   | Q     | 0.657 | 8.1                   | 1.4                            | 17.0     | 6.0             | 14.48                | 6            | 9           | 4.85        | 1     |
| J2025–0735      | PKS2022–077  | Q     | 1.388 | 16.5                  | 4.9                            | 24.6     | 3.3             | 23.20                | 7            | 9           | 2.64        | 2     |
| J2143+1743      | PKS2141+175  | Q     | 0.213 | 8.8                   | 1.8                            | 4.7      | 3.0             | 2.15                 | 8            | 9           | 2.64        | 2     |
| J2147+0929      | 2144+092     | Q     | 1.113 | 13.6                  | 1.8                            | –        | –               | –                    | 5            | 9           | 2.64        | 2     |
| J2202+4216      | 2200+420     | B     | 0.069 | 6.1                   | 0.8                            | 5.6      | 9.4             | 5.49                 | 12           | 9           | 2.64        | 2     |
| J2203+1725      | PKS2201+171  | Q     | 1.076 | 10.0                  | 0.5                            | 8.4      | 5.7             | 8.17                 | 4            | 9           | 8.35        | 0     |
| J2203+3145      | 2201+315     | Q     | 0.295 | 4.1                   | 1.1                            | 6.3      | 13.2            | 5.79                 | 8            | 5           | 23.05       | 0     |
| J2229–0832      | 2227–088     | Q     | 1.560 | 21.0                  | 0.6                            | 10.6     | 0.5             | 1.92                 | 5            | 9           | 4.85        | 1     |
| J2232+1143      | 2230+114     | Q     | 1.037 | 15.1                  | 4.8                            | 8.1      | 1.9             | 4.00                 | 8            | 9           | 4.85        | 1     |
| J2253+1608      | 2251+158     | Q     | 0.859 | 17.0                  | 3.7                            | 10.4     | 2.6             | 7.90                 | 7            | 10          | 42.00       | 2     |
| J2327+0940      | PKS2325+093  | Q     | 1.841 | 17.2                  | 2.3                            | –        | –               | –                    | 6            | 9           | 4.85        | 2     |

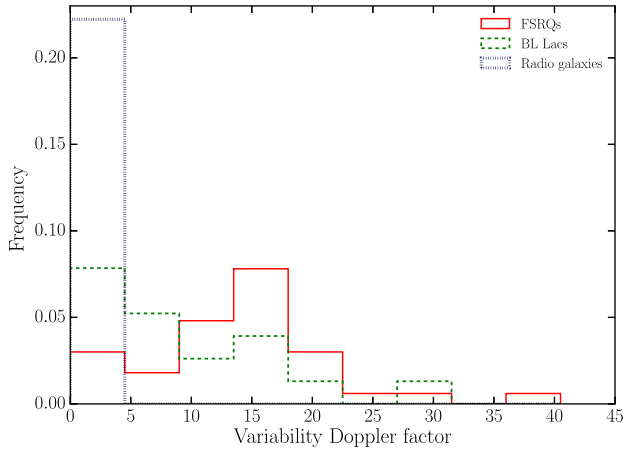


**Figure 3.** Distribution of the variability Doppler factor for the F-GAMMA sources. Solid red is for FSRQs, dashed green for BL Lacs and dotted blue for radio galaxies in our sample.

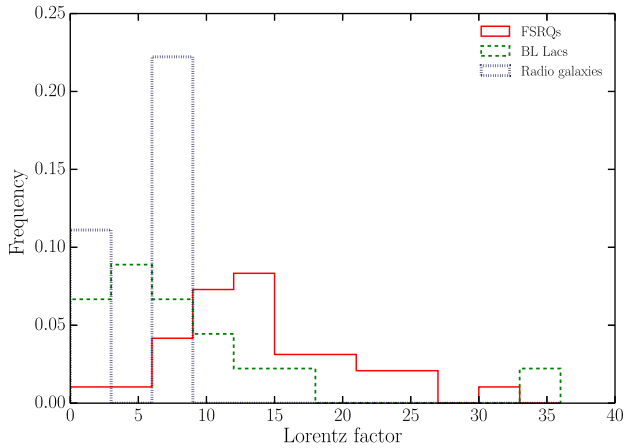


**Figure 4.** Distribution of the Lorentz factor for the F-GAMMA sources. Solid red is for FSRQs, dashed green for BL Lacs and dotted blue for radio galaxies in our sample.

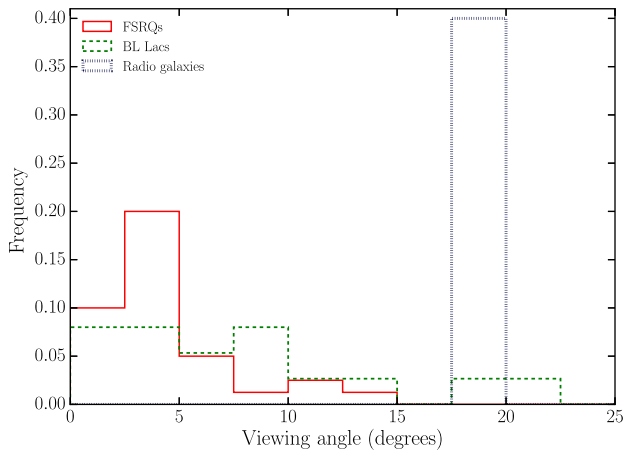


**Figure 5.** Distribution of the viewing angle for the F-GAMMA sources. Solid red is for FSRQs, dashed green for BL Lacs and dotted blue for radio galaxies in our sample.

**Table 2.** Mean and standard deviation (std) of Doppler factors, Lorentz factors and viewing angles for the three populations in our sample.

|                                 | FSRQ  | BL Lacs | Radio galaxies |
|---------------------------------|-------|---------|----------------|
| $\delta_{\text{var}}$           |       |         |                |
| mean                            | 15.21 | 9.2     | 1.4            |
| std                             | 8.7   | 7.6     | 0.8            |
| $\Gamma_{\text{var}}$           |       |         |                |
| mean                            | 13.9  | 9.2     | 5.2            |
| std                             | 6.1   | 8.8     | 2.2            |
| $\theta_{\text{var}}$ (degrees) |       |         |                |
| mean                            | 4.2   | 7.8     | 22.2           |
| std                             | 2.9   | 6.1     | 3.3            |

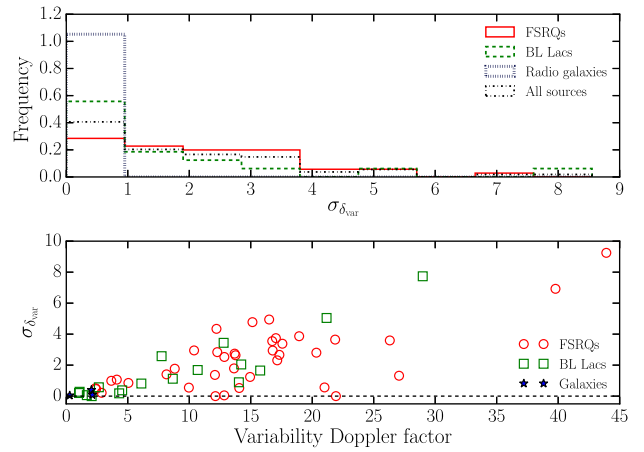


**Figure 6.** *Upper panel:* distribution of error estimates of the variability Doppler factor for the F-GAMMA sources. Solid red is for FSRQs, dashed green for BL Lacs, dotted blue for radio galaxies and black dash-dotted for the whole sample. *Lower panel:* variability Doppler factor versus the error of each estimate. Red circles are for FSRQs, green squares for BL Lacs and blue stars for radio galaxies.

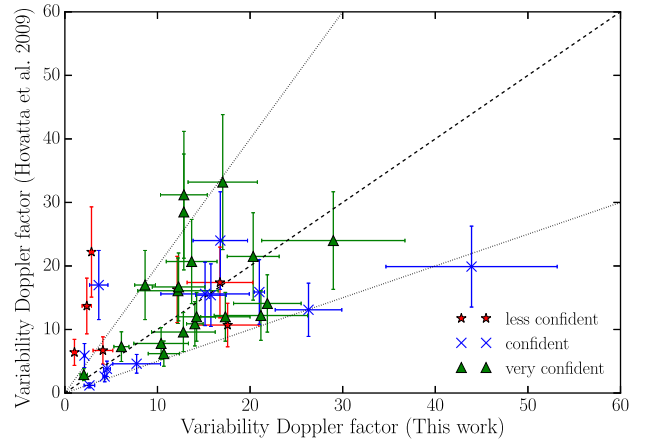


**Figure 7.** Variability Doppler factors (this work) versus variability Doppler factors from Hovatta et al. (2009). The green triangle denotes sources for which we are very confident of our analysis, blue x sources for which we are confident and red star sources for which we are less confident (see Table 1). The dashed line denotes the  $y = x$  line, whereas the dotted lines mark the factor-of-two envelope. The error of the y-axis is the 30 per cent average error derived through population modelling.

exact error in  $\delta_{\text{var}}$ . They provide an upper limit on the error in their estimates by calculating the standard deviation of the different  $\delta_{\text{var}}$  for individual well-defined flares in each source. They find a median standard deviation of  $\sim 27$  per cent. However, population models find that the error in their estimates on average is  $\sim 30$  per cent. The error of the y-axis is the  $\sim 30$  per cent average error derived from population modelling (Liodakis & Pavlidou 2015b).

Although there are some discrepancies, the majority of the estimates are within the factor-of-two envelope and most are within errors. The two-sample Kolmogorov–Smirnov test (K–S test) yielded a 69.25 per cent probability of consistency between the estimates of the two methods (the null hypothesis is that the two samples are drawn from the same population). Testing for their correlation, the Spearman rank-order correlation yielded a correlation coefficient  $r = 0.5$  ( $-1$  negative correlation,  $0$  no correlation,  $1$  positive correlation) with a  $\sim 0.1$  per cent probability of the two samples being uncorrelated. Excluding the estimates for which we are less confident in our analysis, the K–S test yielded a 94.4 per cent probability of consistency and the Spearman rank-order  $r = 0.57$ , with  $\sim 0.08$  per cent probability of uncorrelated samples. Thus we can conclude that the estimates of the two methods are drawn from the same population.

Our method tends to yield higher estimates of the Doppler factors than Hovatta et al. (2009), although this is not confirmed by the Wilcoxon rank-sum test (41.18 per cent). This trend is more prominent at high values of the Doppler factor, which is to be expected, since in our approach the effects of cadence of observations are mitigated. On the other hand, there are sources for which our estimates are lower. Although some of these estimates fall under our ‘less confident’ category, there are sources for which we are confident in our results. A possible explanation for this discrepancy would be the uncertainty in the estimates in Hovatta et al. (2009). For example, an inadequate fit or fitting what would appear as a flaring event but is instead stochastic variability could lead to underestimation of the time-scale and consequently overestimation of the Doppler factor. A more probable scenario, given the span (roughly  $\sim 35$  years) of the Metsähovi monitoring programme, would be the occurrence of a major flare in each of these sources outside the F-GAMMA monitoring period. This could lead to higher brightness temperatures and hence higher Doppler factors for these sources. The origin of this discrepancy needs to be investigated on the basis of a source-by-source analysis, which is currently in progress. In any case, inconsistencies only concern nine sources. Their impact on the results of this study is therefore very low.

## 5 SUMMARY

We used specially designed algorithms in order to identify, track and characterize flares over a large number of radio frequencies from 2.64 up to 142.33 GHz with data from the F-GAMMA blazar monitoring programme (Fuhrmann et al. 2007, 2016; Angelakis et al. 2010, 2012). Using the variability brightness temperature obtained with this approach (Angelakis et al. 2015), we were able to calculate the variability Doppler factor (equation 2) for 58 sources, for 20 of which no variability Doppler factor had been estimated before, and provide error estimates on a source-by-source basis. Combined with apparent velocities from the MOJAVE survey (Lister & Homan 2005), we calculated the Lorentz factor and viewing angles for 50 sources. All values, as well as additional information on the sources, are listed in Table 1. Our results can be summarized as follows.

(i) There are differences in the Doppler factor estimates between the BL Lacs and FSRQs. FSRQs appear to have significantly larger Doppler factors and Lorentz factors and smaller viewing angles, consistent with our current understanding of blazars (Jorstad et al. 2005; Hovatta et al. 2009; Lister et al. 2013; Liodakis & Pavlidou 2015a).

(ii) Both FSRQ and BL Lac populations have higher Doppler and Lorentz factors than radio galaxies. The viewing angles are typically  $< 15^\circ$  for all blazars except one BL Lac object, whereas radio galaxies have viewing angles  $\geq 20^\circ$ , consistent with our current view on the unification of radio galaxies (Ghisellini et al. 1993; Urry & Padovani 1995).

(iii) The mean error of our estimates is 2.07. Our highest percentage error (35.5 per cent) is comparable with the most accurate estimates available in the literature (30 per cent on average, Hovatta et al. 2009), whereas our average error is 16 per cent. Thus, our method is the most accurate for estimating the Doppler factor of blazar jets to date, with the unique ability to provide error estimates on a source-by-source basis.

(iv) We compared the Doppler factors derived from this work with estimates from the literature (Hovatta et al. 2009) that have been shown to describe blazar populations adequately (Liodakis & Pavlidou 2015b). There are very few discrepancies, which can be attributed to uncertainties in either the analysis of the literature values or the analysis presented here. Nevertheless, the two samples are consistent within the errors, as is validated confidently by the Kolmogorov–Smirnov and Spearman rank-order correlation tests.

The multiwavelength variability Doppler factors presented here were found to be consistent with the estimates in Hovatta et al. (2009), which can describe the FSRQ and BL Lac populations adequately (Liodakis & Pavlidou 2015b). Hence, we can conclude that they not only are the most accurate estimates yet, but can also describe blazars as a population, validating our results and stressing the importance and wealth of information that can be obtained from multiwavelength monitoring programmes such as F-GAMMA.

## ACKNOWLEDGEMENTS

The authors thank Talvikki Hovatta, Shoko Koyama and the anonymous referee for comments and suggestions that helped improve this work. This research was supported by the ‘Aristeia’ Action of the ‘Operational Program Education and Lifelong Learning’ and is co-funded by the European Social Fund (ESF) and Greek National Resources, and by the European Commission Seventh Framework Program (FP7) through grants PCIG10-GA-2011-304001 ‘JetPop’ and PIRSES-GA-2012-31578 ‘EuroCal’. This research has made use of data from the MOJAVE data base, which is maintained by the MOJAVE team (Lister et al. 2009). Our study is based on observations carried out with the 100-m telescope of the MPIfR (Max-Planck-Institut für Radioastronomie) and the IRAM 30-m telescope. IRAM is supported by INSU/CNRS (France), MPG (Germany) and IGN (Spain). IN, IM and VK were supported for this research through a stipend from the International Max Planck Research School (IMPRS) for Astronomy and Astrophysics at the Universities of Bonn and Cologne.

## REFERENCES

- Acero F. et al., 2015, *ApJS*, 218, 23
- Angelakis E., Fuhrmann L., Nestoras I., Zensus J. A., Marchili N., Pavlidou V., Krichbaum T. P., 2010, preprint ([arXiv:1006.5610](https://arxiv.org/abs/1006.5610))

- Angelakis E. et al., 2012, J. Phys. Conf. Ser., 372, 012007  
 Angelakis E. et al., 2015, A&A, 575, A55  
 Blandford R. D., Königl A., 1979, ApJ, 232, 34  
 Dondi L., Ghisellini G., 1995, MNRAS, 273, 583  
 Edelson R. A., Krolik J. H., 1988, ApJ, 333, 646  
 Fuhrmann L., Zensus J. A., Krichbaum T. P., Angelakis E., Readhead A. C. S., 2007, in Ritz S., Michelson P., Meegan C. A., eds, AIP Conf. Ser. Vol. 921, The First GLAST Symposium. Am. Inst. Phys., New York, p. 249  
 Fuhrmann L. et al., 2016, A&A, 596, A45  
 Ghisellini G., Padovani P., Celotti A., Maraschi L., 1993, ApJ, 407, 65  
 Gujosa A., Daly R. A., 1996, ApJ, 461, 600  
 Hovatta T., Valtaoja E., Tornikoski M., Lähteenmäki A., 2009, A&A, 494, 527  
 Jorstad S. G. et al., 2005, AJ, 130, 1418  
 Jorstad S. G. et al., 2006, in Miller H. R., Marshall K., Webb J. R., Aller M. F., eds, ASP Conf. Ser. Vol. 350, Blazar Variability Workshop II: Entering the GLAST Era. Astron. Soc. Pac., San Francisco, p. 149  
 Kellermann K. I., Pauliny-Toth I. I. K., 1969, ApJ, 155, L71  
 Komatsu E. et al., 2009, ApJS, 180, 330  
 Lähteenmäki A., Valtaoja E., 1999, ApJ, 521, 493  
 Lähteenmäki A., Valtaoja E., Wiik K., 1999, ApJ, 511, 112  
 Lehar J., Hewitt J. N., Burke B. F., Roberts D. H., 1992, ApJ, 384, 453  
 Liodakis I., Pavlidou V., 2015a, MNRAS, 451, 2434 (Paper I)  
 Liodakis I., Pavlidou V., 2015b, MNRAS, 454, 1767  
 Lister M. L., Homan D. C., 2005, AJ, 130, 1389  
 Lister M. L. et al., 2009, AJ, 138, 1874  
 Lister M. L. et al., 2013, AJ, 146, 120  
 Mattox J. R. et al., 1993, ApJ, 410, 609  
 Readhead A. C. S., 1994, ApJ, 426, 51  
 Richards J. L. et al., 2011, ApJS, 194, 29  
 Urry C. M., Padovani P., 1995, PASP, 107, 803  
 Valtaoja E., Lähteenmäki A., Teräsanta H., Lainela M., 1999, ApJS, 120, 95

## APPENDIX A: VARIABILITY DOPPLER FACTOR DERIVATION

We use the expression for the variability brightness temperature (equation A1) from Blandford & Königl (1979) and equations (A2) and (A3) in order to obtain the correct expression for the variability Doppler factor:

$$T_{\text{var}} = \frac{D_L^2 \Delta S_{\text{ob}}(\nu)}{2\nu^2 t_{\text{var}}^2 k(1+z)^4}, \quad (\text{A1})$$

$$I(\nu) = \frac{2k\nu^2 T_{\text{var}}}{c^2} = \frac{\Delta S(\nu)}{\theta^2}, \quad (\text{A2})$$

$$\frac{I'(\nu)}{\nu^3} = \frac{I(\nu)}{\nu^3}, \quad (\text{A3})$$

where  $T_{\text{var}}$  is the variability brightness temperature,  $D_L$  the luminosity distance,  $\nu$  the frequency,  $t_{\text{var}}$  the variability time-scale,  $z$  the

redshift,  $I(\nu)$  the intensity,  $k$  Boltzman's constant,  $c$  the speed of light,  $\Delta S(\nu)$  the flux density and  $\theta$  the angular size of the source. Primed symbols denote rest-frame quantities. Combining equations (A1) and (A2),

$$T_{\text{var}} = \frac{D_L^2 I(\nu) \theta^2}{2\nu^2 t_{\text{var}}^2 k(1+z)^4}. \quad (\text{A4})$$

The observed transverse size is

$$R = \frac{\delta_{\text{var}} c t_{\text{var}}}{1+z} = D_A \theta \Rightarrow \theta = \frac{\delta_{\text{var}} c t_{\text{var}}}{D_A(1+z)}, \quad (\text{A5})$$

where  $D_A$  is the angular diameter distance to the source and  $\delta_{\text{var}}$  the Doppler factor. From equation (A3), we have that  $I(\nu) = \delta_{\text{var}}^3 I'(\nu)$ . If we take cosmological expansion into account,  $I(\nu) = \delta_{\text{var}}^3 I'(\nu)(1+z)^{-3}$  (because  $\nu' = (1+z)\nu$ ). Putting everything in equation (A4), then,

$$T_{\text{var}} = \frac{D_L^2 I(\nu)}{2\nu^2 t_{\text{var}}^2 k(1+z)^4} \left( \frac{\delta_{\text{var}} c t_{\text{var}}}{D_A(1+z)} \right)^2. \quad (\text{A6})$$

The angular diameter distance is defined as  $D_A = D/(1+z)$  and the luminosity distance as  $D_L = D(1+z) \Rightarrow D^2 = D_L^2/((1+z)^2)$ . The variability brightness temperature becomes

$$\begin{aligned} T_{\text{var}} &= \frac{c^2}{2k} \frac{D^2 I(\nu)}{\nu^2 t_{\text{var}}^2 (1+z)^2} \frac{\delta_{\text{var}}^2 c^2 t_{\text{var}}^2}{D^2} \\ &= \frac{c^2}{2k} \frac{I(\nu)}{\nu^2 (1+z)^2} \delta_{\text{var}}^2 c^2 \\ &= \frac{c^2}{2k} \frac{I'(\nu) \delta_{\text{var}}^3 \delta_{\text{var}}^2}{\nu^2 \delta_{\text{var}}^2 (1+z)^3 (1+z)^2 (1+z)^{-2}} \\ &= \frac{c^2 I'(\nu)}{2k \nu^2} \frac{\delta_{\text{var}}^3}{(1+z)^3} = \frac{\delta_{\text{var}}^3}{(1+z)^3} T_{\text{var}}'. \end{aligned} \quad (\text{A7})$$

Assuming that, while flaring, the source reaches equipartition between the energy density of the magnetic field and that of the radiating particles (Readhead 1994), we can substitute the intrinsic brightness temperature with the equipartition brightness temperature ( $T_{\text{eq}} = 5 \times 10^{10}$  K):

$$T_{\text{var}} = \frac{\delta_{\text{var}}^3}{(1+z)^3} T_{\text{eq}}. \quad (\text{A8})$$

The variability Doppler factor will be

$$\delta_{\text{var}} = (1+z) \sqrt[3]{\frac{T_{\text{var}}}{T_{\text{eq}}}}. \quad (\text{A9})$$

This paper has been typeset from a  $\text{\LaTeX}$  file prepared by the author.